Catalytic Formation of Narrow Nb Nanowires inside Carbon Nanotubes

Dan Liu, David Tománek*

Physics and Astronomy Department, Michigan State University, East Lansing, Michigan 48824, USA

Abstract

We propose a previously unexplored way to form Nb nanowires from $NbCl_3$ molecules inside carbon nanotubes (CNTs). We have studied this reaction by *ab initio* density functional calculations and found it to be catalytically promoted in presence of graphitic carbon. Our results suggest that chemisorption of $NbCl_3$ on the CNT is accompanied by a charge transfer of ≈ 0.5 electrons to the nanotube wall, which significantly weakens the Nb-Cl bond. We found that the bcc structure of Nb is not affected by the small diameter of the nanowire inside a CNT. We have also identified strong covalent bonds between the nanowires and the surrounding nanotube that are accompanied by a similar charge transfer of $\lesssim 0.5$ e from surface Nb atoms to the nanotube. The large electronic density of states of bulk Nb at E_F is not changed much in the confined geometry, suggesting that ultra-narrow nanowires of Nb may keep their superconducting behavior and form Josephson junctions in the quasi-1D geometry while being protected from the ambient by the enclosing CNT structure.

Keywords: Nanotube, carbon, CNT, catalyst, niobium, nanowire, superconductor, DFT

1. Introduction

Niobium holds a special place in the periodic table for several reasons. It is a ductile transition metal with a high melting temperature [1] T_M = 2750 K and the highest cohesive energy [1] E_{coh} = 7.57 eV/atom in the $4d$ transition metal series. Nb also displays the highest critical temperature T_c = 9.25 K among elemental superconductors [2, 3] and is unique with its ability to maintain an open body-centered cubic (bcc) structure until extremely high pressures [4] of hundreds of GPa. Nb is significantly harder than iron and an important constituent of thermally stable superalloys and superconducting alloys. There is strong interest in Nb nanowires covering applications ranging from efficient superconducting single-photon detectors [5, 6], Josephson tunnel junctions [7], and conductive fiber composites used as supercapacitors [8] and energy storage media [9]. A wide range of fabrication techniques including etching of sputter-deposited films [5] or compounds [9], templated electrodeposition [10], or deposition on nano-templates [11] were only capable of producing polycrystalline wires with diameters from 10-1000 nm. Availability of monocrystalline Nb nanowires with only few nanometers in diameter is highly desirable especially for quantum applications in the superconducting regime. Yet the common synthesis approach based on high-temperature capillarity filling [12–20] of carbon nanotubes can not be used for Nb due to its high melting temperature, which is close to the stability limit of carbon nanotubes.

Here we propose a previously unexplored approach to synthesize Nb nanowires with a uniform diameter by heating up the $NbCl_3$ molecular crystal in presence of carbon nanotubes (CNTs) with a typical diameter $d \lesssim 2$ nm. The nanowires should form by decomposition of $NbCl_3$ inside CNTs at a temperature well below the melting point of Nb. In this process, the role of the CNT is threefold. First, the CNT is a template that defines the diameter of the enclosed. Second, graphitic carbon in the CNT acts as a catalyst, which lowers the temperature of converting $NbCl_3$ to metallic Nb and $NbCl_5$ to well below $1,000°C$ [21]. Finally, the CNT protects the enclosed Nb nanowire from the ambient. We have performed *ab initio* density functional theory (DFT) calculations of the reaction mechanism and found that Nb nanowires may form in an activated exothermic process that involves a large number of atoms in concerted motion. The catalytic effect of a CNT originates in its ability to accept electrons from chemisorbed $NbCl_3$. Our

---
*Corresponding author

Email address: tomanek@pa.msu.edu (David Tománek)

calculations allow us to identify the optimum geometry of Nb nanowires that form inside the CNTs. Nb nanowires are faceted fragments of the bulk bcc structure with little reconstruction. They maintain the same high density of states at E_F as bulk Nb and thus should remain superconducting, similar to their bulk counterpart. More interesting, ultra-narrow Nb nanowire segments, separated by a narrow gap and held in place by the surrounding CNT, should form a Josephson junction in the quasi-1D geometry while being protected from the ambient by the enclosing CNT structure.

At first glance, formation of Nb nanowires inside carbon nanotubes should not appear surprising, since nanowires of other elements have been found inside CNTs[12–20]. So far, filling nanotubes by a metal [12] such as Pb had required initial melting of this metal, which subsequently entered the nanotubes by capillary action. Similar to other refractory metals, this approach fails for Nb with it melting point [1] T_M = 2750 K, which is close to the stability limit of carbon nanotubes between 951 K in presence of oxygen [22] and near 3, 400 K in vacuum [23].

Our proposed approach is very different, as it involves sublimation of NbCl$_3$ molecules from a molecular crystal, their entry into the open end of a CNT and subsequent chemisorption on the inner wall. As we will discuss below, we find that chemisorption of NbCl$_3$ on the CNT wall is accompanied by a large charge transfer of 0.5 electrons from the molecule to the CNT, which strongly reduces the ionic charge of Cl atoms in this molecule. The charge redistribution in the adsorbed complex lowers the energy required to break the Nb-Cl bond by $\gtrsim$1 eV. Consequently, the exothermic conversion of NbCl$_3$ to metallic Nb and NbCl$_5$ is promoted in presence of graphitic carbon, which plays the unusual role of a catalyst. There is preliminary experimental evidence [24] that formation of Nb nanowires inside CNTs from NbCl$_3$ is indeed possible at temperatures significantly lower than 1, 000°C, which is required for this reaction to occur in vacuum, without a catalyst [21].

2. Computational results

We have considered different chlorides of niobium as potential precursors for metallic Nb and calculated the corresponding reaction energies by optimizing the initial and the final structures using *ab initio* DFT calculations. Among these, we found NbCl$_5$ to be unusually stable, as it forms spontaneously from metallic Nb and chlorine gas according to [25]
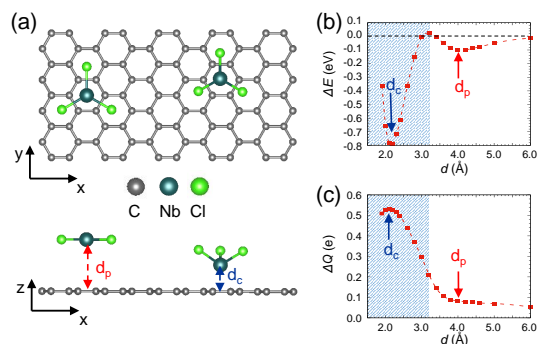
$$\text{Nb(s)} + 2.5\text{Cl}_2\text{(g)} \longrightarrow \text{NbCl}_5\text{(s)} . \qquad (1)$$

Figure 1: Interaction of an NbCl$_3$ molecule with a graphene monolayer. (a) Side and top views of the molecule at the distance $d = d_c$ and $d = d_p$ from graphene. (b) Interaction energy $\Delta E(d)$ between an NbCl$_3$ molecule and graphene. (c) Charge redistribution upon chemisorption of NbCl$_3$ on graphene.

The observed reaction energy [25, 26] of −797 kJ/mol or −8.26 eV per formula unit is in fair agreement with the calculated value of −7.48 eV. The strongly exothermic nature of this process indicates that the reverse process of forming metallic Nb from NbCl$_5$ is highly unlikely.

However, we found metallic Nb to form as one of the products of the decomposition of NbCl$_3$ according to [21, 27]

$$5\text{NbCl}_3\text{(s)} \longrightarrow 3\text{NbCl}_5 + 2\text{Nb(s)} . \qquad (2)$$
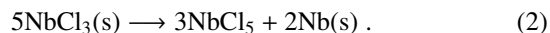
This reaction is exothermic and has been reported to occur at 1, 000°C under vacuum conditions [21, 27]. Even though NbCl$_5$ molecules are listed as one of the products, these molecules are known to dimerize spontaneously to Nb$_2$Cl$_{10}$. Then, Eq. (2) changes to

$$10\text{NbCl}_3\text{(s)} \longrightarrow 3\text{Nb}_2\text{Cl}_{10}\text{(g)} + 4\text{Nb(s)} . \qquad (3)$$
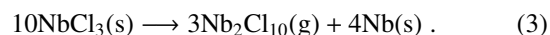
The calculated reaction energy of this exothermic process is ΔE = −19.82 eV. Even though we know that this reaction does occur at 1, 000°C, there is only limited information available about it due to its complexity [28], which involves continuous changes in the oxidation state of Nb. The reaction involves a concerted motion of 40 atoms in a 120-dimensional configuration space that is hard to search. Consequently, the reaction coordinate and transition states can not be characterized well, as we expand on in the Supplementary Material (SM).

According to Eq. (3), we consider NbCl$_3$ as a suitable precursor for the formation of metallic Nb. We note that this favorable precursor may also form by exposing NbCl$_5$ to hydrogen atmosphere according to [27]

$$\text{NbCl}_5\text{(g)} + \text{H}_2\text{(g)} \longrightarrow \text{NbCl}_3\text{(s)} + 2\text{HCl(g)} . \qquad (4)$$

This reaction is only slightly exothermic, with the reported reaction energy [27] of -35 kJ/mol. Even though we are unable to characterize the reaction coordinate, transition states and activation energies for the reaction in Eq. (3), we are still able to shed light on key steps in the reaction, which involves breaking of some and formation of other bonds in the Nb-Cl system, leading ultimately to metallic Nb inside a CNT.

In the first step, an $NbCl_3$ molecule adsorbs on the inner wall of the CNT, which we represent by a graphene monolayer in view of the low curvature of the 2-nm wide CNT. Our results are summarized in Fig. 1. Corresponding results for the interaction of $NbCl_5$ with graphene are presented in the SM.

As seen in Fig. 1(a), $NbCl_3$ is a planar molecule that prefers adsorption in the hollow site on graphene. The adsorption energetics is depicted in Fig. 1(b). $NbCl_3$ initially physisorbs at the distance $d_p = 4.07$ Å, gaining 0.10 eV in physisorption energy. Only a small energy barrier separates it from a much more stable chemisorbed state associated with an energy gain of 0.80 eV and a much smaller distance $d_c = 2.15$ Å from graphene. As shown in Fig. 1(a), the molecule deforms during the chemisorption, bringing the Nb atom closer to the surface. To better understand the changes in chemical bonding associated with the adsorption of $NbCl_3$ on graphene, we performed a single$-\zeta$ Mulliken population analysis of the system and monitored the net charge Q of $NbCl_3$ at different values of the adsorption distance d. We then defined the electron depletion $\Delta Q(d)$ on the molecule at distance d with respect to a desorbed molecule at $d = 10$ Å by $\Delta Q(d) = Q(d = 10$ Å$) - Q(d)$. Our results in Fig. 1(c) indicate that the molecule remains almost neutral down to $d = d_p$, but loses up to 0.53 electrons as it approaches graphene in the chemisorbed state. From this viewpoint, graphene is not inert with respect to the chemical behavior of $NbCl_3$.

As mentioned above, formation of metallic Nb from $NbCl_3$ molecules during the complex reaction behind Eq. (3) necessitates breaking or rearranging Nb-Cl bonds. Whereas separating a Cl atom from a free $NbCl_3$ molecule requires 4.57 eV, the same process requires only 2.60 eV when $NbCl_3$ is chemisorbed on graphene or inside a CNT. Also a related endothermic reaction that is likely to occur during the complex conversion process, where $NbCl_3$ first dimerizes to Nb_2Cl_6 and subsequently dissociates into $NbCl_2$ and $NbCl_4$, requires 1.26 eV in vacuum and a significantly lower energy of 0.52 eV while adsorbed on graphitic carbon of a nanotube. Details of these particular reactions are presented in the SM.

We attribute the significant decrease of the reaction

energy barriers on graphitic carbon to the electron transfer from the chemisorbed molecule to the carbon nanotube. This catalytic effect is unusual, since with few exceptions [29, 30], graphitic carbon has been known to be catalytically inactive unless combined with another substance to form a graphene-based catalyst or a supported graphene catalyst. Consequently, formation of metallic Nb from $NbCl_3$ according to the reaction in Eq. (3) should occur inside a CNT at temperatures significantly lower than the reported value of $1,000°C$ in vacuum [21, 27]. This conjecture appears to be supported by preliminary experimental results [24].

Having established the possibility of forming metallic Nb inside a CNT, we now have to consider likely structures of finite-diameter Nb nanowires that are dynamically stable. Unlike in macroscopic structures including large-diameter wires, atomic packing may be significantly changed in nanostructures including nanowires due to the significant effect of surface tension that exerts compressive stress on the entire structure. We summarize observed and calculated values of the surface tension γ in Table 1. We have estimated the equivalent pressure for Nb nanowires in excess of 2 nm diameter and found it insufficient to convert the open bcc structure of bulk Nb to a more close-packed structure, in agreement with previous results [4]. We also cut out and optimized selected nanowires from bulk Nb(bcc) and found no signs of significant reconstruction. Thus, we believe that same as in the bulk, atoms in Nb nanowires are packed in the bcc structure, with possible atomic relaxations at the surface. The nanowires discussed in the following are to be considered stable dynamically, not only statically, since atomic rearrangement to a more stable structure has been excluded. Still, there is need to discuss possible shape changes at their faceted surface inside the nanotube void, which we do in the following.

Whereas the most stable structure would minimize the total surface energy in vacuum, it should minimize the total interface energy between Nb and the CNT in the Nb@CNT system. To obtain insight into the different components of the interface energy, we do not constrain our study to particular nanotube diameters, but rather study different Nb surfaces and their interaction with a graphene monolayer.

As a likely candidate for segments of the nanowire surface, we first consider the Nb(110) surface with the lowest value of γ according to Table 1. We would expect Nb nanowires with a surface consisting only of (110) facets to be most stable in vacuum. The interaction of the Nb(110) surface with graphene, representing a finite-diameter nanowire enclosed in a CNT, is presented in Fig. 2. Corresponding results for the Nb(100),
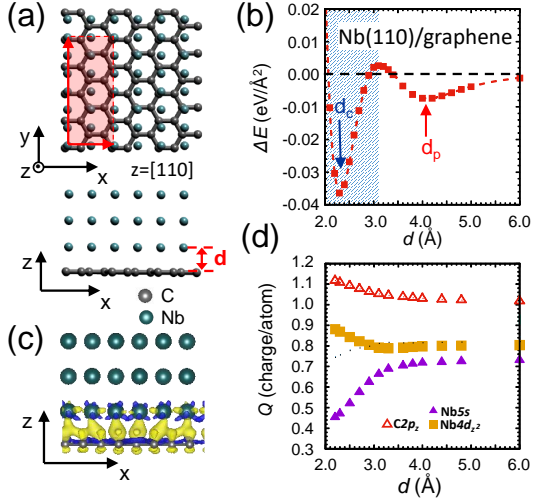
Figure 2: Interaction of the Nb(110) surface with a graphene mono-layer. (a) Top and side views of the atomic arrangement, with the supercell highlighted by red. (b) Interaction energy ΔE between the Nb(110) surface and graphene as a function of the separation distance d. (c) Charge redistribution caused by the interaction of Nb(110) with graphene, superposed with the atomic structure. $\Delta\rho = \rho(\text{Nb/graphene}) - \rho(\text{Nb}) - \rho(\text{graphene})$ is shown by isosurfaces bounding regions of electron excess at $+4\times10^{-3}$ e/Å^3 (yellow) and electron deficiency at -4×10^{-3} e/Å^3 (blue). (d) Mulliken charge of specific atomic orbitals as a function of d.

Nb(111) and Nb(121) surfaces are presented in the SM. We represent the Nb(110) surface by a 3-layer slab.

Table 1: Characterization of selected Nb surfaces and their interaction with graphene based on DFT-PBE calculations. γ is the surface energy. The optimum Nb-graphene distance is d_c for chemisorption and d_p for physisorption. $\Delta E(d_c)$ is the Nb-graphene interaction energy and $\Delta Q(d_c)$ is the electron charge transferred from Nb to graphene at d_c, both given per area unit.

Surface	γ (eV/Å^2)	d_c (Å)	d_p (Å)	$\Delta E(d_c)$ (eV/Å^2)	$\Delta Q(d_c)$ (e/Å^2)
(100)	0.152	2.32	-	0.035	0.040
	0.142[a]				
(110)	0.127	2.31	4.07	0.037	0.048
	0.129[a]				
	0.155[b]				
	0.159[c]				
(111)	0.150	2.28	-	0.022	0.031
	0.146[a]				
(121)	0.146	2.37	-	0.025	0.032
	0.146[a]				

[a] Ref. [31].
[b] Ref. [32].
[c] Ref. [33].

Since Nb(110) is not epitaxial with the honeycomb lattice of graphene, we considered a large Nb$_{18}$C$_{16}$ supercell depicted in Fig. 2(a), which contained 16 C and 6 Nb atoms at the interface. Epitaxy, needed for the calculation, was enforced by compressing Nb(110) by 0.8% along the x-direction and stretching it by 2.1% along the y-direction, whereas graphene was left in its optimum structure. The Nb(110)/graphene interaction energy ΔE is plotted in Fig. 2(b) as a function of the interface distance d. Similar to the NbCl$_3$ molecule on graphene discussed above, we find two adsorption minima for this system. As also listed in Table 1, the shallower minimum, which we associate with physisorption, is characterized by $d_p = 4.07$ Å and $\Delta E_p = -0.008$ eV/Å^2. The deeper minimum, which we associate with chemisorption, is characterized by $d_c = 2.31$ Å and $\Delta E_c = -0.037$ eV/Å^2. These interaction energies are smaller than the surface energies listed in Table 1, but can not be ignored when discussing the surface structure of nanowires inside a CNT.

We find similarities in the interaction of graphene with the surface of Nb and a NbCl$_3$ molecule. Unlike in the physisorbed state of Nb on graphene, there is significant electron transfer from Nb to graphene in the more stable chemisorbed state. The spatial extent of this charge transfer is, however, limited to the one Nb layer closest to graphene, as shown in Fig. 2(c). To better understand the details of this charge transfer, we plotted the Mulliken population charge, obtained using a single-ζ basis, in Fig. 2(d) for atomic orbitals that were most affected. In graphene, it was the population of the C2p_z orbital that increased at smaller interlayer distances. In Nb, the population of the Nb4d_{z^2} state increased and that of the Nb5s state decreased significantly at small interlayer distances. This confirms that the most significant bonding between Nb and C is associated with $pd\sigma$ bonding gaining strength over the $sp\sigma$ bond as Nb and C atoms approach each other. This bonding character is also reflected in the charge density redistribution in Fig. 2(c).

The interaction energies of different Nb surfaces with graphene are compared in Figs. 3(a)-3(c). Unlike for the (110) surface discussed above, there are no physisorption minima for Nb(100) and Nb(121) interacting with graphene. Among the three surfaces considered, Nb(110) interacts most strongly with graphene. The numerical values for the interaction energies of the different surfaces with graphene are summarized in Table 1.

Candidate structures for the most stable, ≈ 2 nm-wide Nb nanowires are shown in Figs. 3(d)-3(f). Of these, the structure in Fig. 3(f) with a hexagonal cross-section
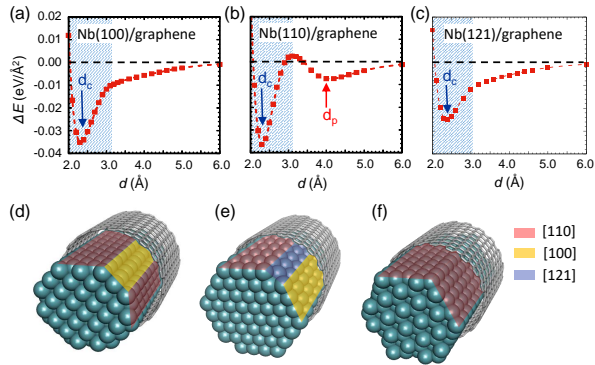
Figure 3: Interaction energy of (a) Nb(100), (b) Nb(110), and (c) Nb(121) with a graphene monolayer. These surfaces form facets on monocrystalline Nb nanowires. Most stable Nb nanowire geometries are shown schematically for nanowires with (d) (100) and (110), (e) (110), (121) and (100), and (f) only (110) facets.
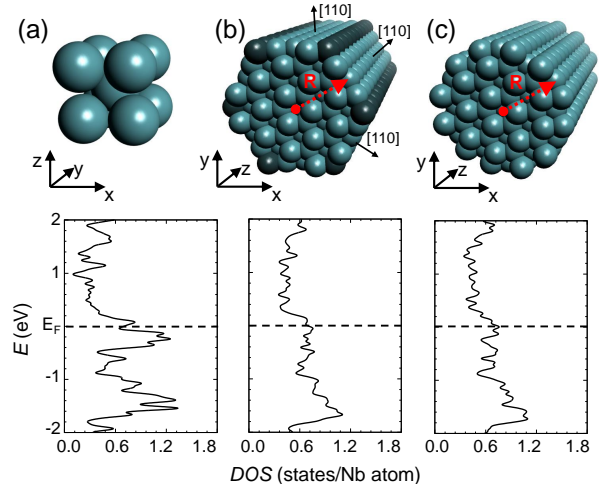

Figure 4: Electronic density of states (DOS) of (a) bulk Nb(bcc), (b) a Nb nanowire terminated by (110) facets, and (c) the Nb nanowire of (b) with atoms at the edges of the facets eliminated.

is the most stable in vacuum, as it is terminated by [110] facets only. Since the Nb(110) surface interacts most strongly with graphene, this structure is favored even more strongly inside a CNT on energy grounds. In nanowires shown in Figs. 3(d) and 3(e), less stable [100] and [121] facets coexist with [110] facets, making these structures energetically less favorable in vacuum than that in Fig. 3(f). Since also the interaction of [100] and [121] facets with graphene is weaker than that of [110] facets, these structures remain energetically less favorable with respect to the structure in Fig. 3(f) also inside a CNT. We thus focus on the preferred structure in Fig. 3(f) in the following.

Finally, to estimate transport properties of Nb nanowires, we compare their electronic density of states (DOS) $N(E)$ to the infinite bcc structure in Fig. 4. We display schematically the bulk bcc structure in the top panel of Fig. 4(a), that of the nanowire of Fig. 3(f) in Fig. 4(b), and the same structure with edge atoms removed in Fig. 4(c). The DOS in the bottom panel of Fig. 4(a) reveals the metallic character of bulk Nb and reflects well the partial filling of the Nb4d band. The DOS of the two nanowires, shown in the bottom panels of Figs. 4(b) and 4(c) appears flatter near the Fermi level. Interestingly, the DOS value at E_F, $N(E_F)$, is essentially the same, possibly slightly higher in the nanowires than in the bulk structure. This would indicate that the conductivity of the nanowires should remain comparable to the bulk structure. We expect an electron transfer from the nanowires to the enclosing nanotube that involves only the outermost atoms in the nanowire. Depending on the nanowire diameter, the position of the Fermi level should be lowered

by $\lesssim 0.1$ eV with no effect on $N(E_F)$. The CNTs surrounding the nanowires may be intrinsically semiconducting or metallic and will contribute negligibly to the conductance of the system. In random samples, 2/3 of all single-wall CNTs are semiconducting.

Possibly more interesting than conducting behavior is the expected change in the critical temperature T_c for superconductivity. In BCS superconductors including Nb, T_c can be estimated using the McMillan equation [34]. The key quantities determining T_c are the the Debye frequency ω_D and the electron-phonon coupling constant λ. Since the structure of the nanowires is essentially the same as that of their bulk counterpart, the vibrational spectra and thus ω_D should be the same. More important are changes in λ, which appears in the exponent of the expression for T_c. One factor in λ, namely the Bardeen-Pines interaction describing electron scattering by a phonon, should be the same in Nb nanowires and bulk Nb due to their similar electronic and phonon structure. The other factor in λ is $N(E_F)$, which we found to be essentially the same, if not higher, in the nanowires of Nb as in the bulk. Thus, we expect Nb nanowires down to 2 nm diameter to remain superconducting, with the same or possibly higher value of T_c than the 9.25 K value [2, 3] reported for bulk Nb.

3. Discussion

The CNTs play a triple role in our study. Besides their catalytic activity to lower the activation barrier for the decomposition of NbCl$_3$ and their function as a template

to form metallic Nb nanowires, they also protect these nanowires from the ambient.

A proper characterization of a chemical reaction involves identifying the reaction coordinate, the geometry and energy of transition states, and a detailed discussion of the dynamical stability of the final state structure. As we mentioned above, the reaction involves a concerted motion of 40 atoms in a 120-dimensional configuration space, which makes it impossible to search for the optimum transformation path between the initial and the final states, which we have characterized. We have also spent significant effort finding the optimum structure of nanowires that fill the void inside a given carbon nanotube. Of course, in absence of this steric constraint, the nanowires would decompose to the bulk Nb(bcc) metal, the most stable structure in the phase diagram of Nb. Clearly, many unknowns remain regrading the reaction details. Still, we have established that due to the catalytic activity of graphitic carbon, the reaction should run below $1,000°$C, at which it had been observed under vacuum conditions.

The complex decomposition reaction of $NbCl_3$ leads not only to metallic Nb, but also to solid $NbCl_5$. The two bulk allotropes of $NbCl_5$ are wide-gap semiconductors and do not affect the electronic properties of the Nb nanowires, as we expand in more detail in the SM. We have also found that the interaction between $NbCl_5$ and the surrounding CNT wall is very weak and does not involve any charge transfer.

In a realistic sample, we may expect that the Nb nanowire may not be contiguous. Rather, finite-length Nb nanowire segments, which are held in place by the surrounding nanotube, may be separated by narrow gaps or short $NbCl_5$ segments along the axial direction of a CNT. Assuming that the surrounding CNT is semiconducting, the Nb-vacuum-Nb or Nb-$NbCl_5$-Nb structure may behave as a nanometer-wide, precisely controllable Josephson junction, the key component of future quantum computers. Besides its nanometer diameter, a significant advantage of a Nb-based Josephoson junction would be its functionality up to T_c(Nb)= 9 K, a significant advantage over Al-based Josephson junctions that only operate below T_c(Al)= 2 K.

4. Summary and Conclusions

We have proposed a previously unexplored way to form Nb nanowires inside carbon nanotubes (CNTs) using not capillary filling by the metal, but rather filling the CNTs with $NbCl_3$ molecules, which decompose to metallic Nb and Nb_2Cl_{10} molecules. We used *ab initio* density functional calculations to get insight into this reaction, which turns out to be quite complex, as it involves a concerted motion of 40 atoms and Nb changing its oxidation state continuously. Whereas the reaction coordinate and associated activation barriers remain obscure, our calculations confirm that the reaction is strongly exothermic. Our finding that particular reaction steps are catalytically promoted in presence of graphitic carbon implies that the reaction temperature should decrease below $1,000°$C required for it to run in vacuum. The same process could be used to form nanowires of other refractory metals including W with an even higher melting point. According to our calculations, chemisorption of $NbCl_3$ on the CNT is accompanied by a charge transfer of $\approx$0.5 electrons to the nanotube wall, which significantly weakens the Nb-Cl bond. We found that the bcc structure of Nb is not affected by the small diameter of the nanowire inside a CNT. We have also identified strong covalent bonds between the nanowires and the surrounding nanotube that are accompanied by a similar charge transfer of $\lesssim$0.5 e from surface Nb atoms to the nanotube. We found that the large electronic density of states at E_F is not changed much in the confined geometry, suggesting that ultra-narrow nanowires of Nb may keep their superconducting behavior in the quasi-1D geometry while being protected from the ambient by the enclosing CNT structure. Under favorable conditions, Nb nanowire segments, separated by narrow gaps, may be held in place by the surrounding nanotube and form Josephson junctions operating at $T \lesssim T_c$(Nb)= 9 K.

5. Computational Techniques

Our calculations of the stability, equilibrium structure and electronic structure have been performed using density functional theory (DFT) as implemented in the SIESTA [35] code. Periodic boundary conditions have been used throughout the study, with 2D slabs or graphene and Nb represented by a periodic array of slabs separated by a 20 Å thick vacuum region. We also used a periodic array to represent 1D Nb nanowires separated by a 15 Å thick vacuum region. We used the Perdew-Burke-Ernzerhof (PBE) [36] exchange-correlation functional. The SIESTA calculations used norm-conserving Troullier-Martins pseudopotentials [37], a double-ζ basis including polarization orbitals, and a mesh cutoff energy of 250 Ry to determine the self-consistent charge density, which provided us with a precision in total energy of $\lesssim$2 meV/atom. The reciprocal space has been sampled by a fine grid [38] of 7×3 k-points in the 2D Brillouin zones (BZ) of the supercells representing Nb/graphene

slabs. The 1D Brillouin zone of Nb nanowires has been sampled by 15 *k*-points. Geometries have been optimized using the conjugate gradient (CG) method [39], until none of the residual Hellmann-Feynman forces exceeded 10^{-2} eV/Å.

Acknowledgments

References

[1] C. Kittel, Introduction to Solid State Physics, 7th Edition, Wiley, 2004.

[2] B. T. Matthias, T. H. Geballe, V. B. Compton, Superconductivity, Rev. Mod. Phys. 35 (1963) 1–22.

[3] D. K. Finnemore, T. F. Stromberg, C. A. Swenson, Superconducting properties of high-purity niobium, Phys. Rev. 149 (1966) 231–243.

[4] P. F. Weck, J. P. Townsend, K. R. Cochrane, S. D. Crockett, N. W. Moore, Shock compression of niobium from first-principles, J. Appl. Phys. 125 (24) (2019) 245905.

[5] A. J. Annunziata, O. Quaranta, D. F. Santavicca, A. Casaburi, L. Frunzio, M. Ejrnaes, M. J. Rooks, R. Cristiano, S. Pagano, A. Frydman, D. E. Prober, Reset dynamics and latching in niobium superconducting nanowire single-photon detectors, J. Appl. Phys. 108 (8) (2010) 084507.

[6] C. M. Natarajan, M. G. Tanner, R. H. Hadfield, Superconducting nanowire single-photon detectors: physics and applications, Supercond. Sci. Technol. 25 (6) (2012) 063001.

[7] M. D. Henry, S. Wolfley, T. Monson, R. Lewis, Ga lithography in sputtered niobium for superconductive micro and nanowires, Appl. Phys. Lett. 105 (7) (2014) 072601.

[8] S. M. Mirvakili, M. N. Mirvakili, P. Englezos, J. D. W. Madden, I. W. Hunter, High-performance supercapacitors from niobium nanowire yarns, ACS Appl. Mater. & Interf. 7 (25) (2015) 13882–13888.

[9] S. M. Mirvakili, A. Pazukha, W. Sikkema, C. W. Sinclair, G. M. Spinks, R. H. Baughman, J. D. W. Madden, Niobium nanowire yarns and their application as artificial muscles, Adv. Funct. Mater. 23 (35) (2013) 4311–4316.

[10] K. Blagg, T. Greymountain, W. Kern, M. Singh, Template-based electrodeposition and characterization of niobium nanowires, Electrochem. Commun. 101 (2019) 39–42.

[11] A. Rogachev, A. Bezryadin, Superconducting properties of polycrystalline nb nanowires templated by carbon nanotubes, Appl. Phys. Lett. 83 (3) (2003) 512–514.

[12] P. M. Ajayan, S. Iijima, Capillarity-induced filling of carbon nanotubes, Nature 361 (6410) (1993) 333–334.

[13] Y. Saito, T. Yoshikawa, Bamboo-shaped carbon tube filled partially with nickel, J. Cryst. Growth 134 (1) (1993) 154–156.

[14] S. C. Tsang, Y. K. Chen, P. J. F. Harris, M. L. H. Green, A simple chemical method of opening and filling carbon nanotubes, Nature 372 (6502) (1994) 159–162.

[15] J. Sloan, D. M. Wright, S. Bailey, G. Brown, A. P. E. York, K. S. Coleman, M. L. H. Green, J. Sloan, D. M. Wright, J. L. Hutchison, H.-G. Woo, Capillarity and silver nanowire formation observed in single walled carbon nanotubes, Chem. Commun. (1999) 699–700.

[16] X. Fan, E. C. Dickey, P. C. Eklund, K. A. Williams, L. Grigorian, R. Buczko, S. T. Pantelides, S. J. Pennycook, Atomic arrangement of iodine atoms inside single-walled carbon nanotubes, Phys. Rev. Lett. 84 (2000) 4621–4624.

[17] G.-H. Jeong, R. Hatakeyama, T. Hirata, K. Tohji, K. Motomiya, T. Yaguchi, Y. Kawazoe, Formation and structural observation of cesium encapsulated single-walled carbon nanotubes, Chem. Commun. (2003) 152–153.

[18] A. García-Fuente, V. M. García-Suárez, J. Ferrer, A. Vega, Structure and electronic properties of molybdenum monatomic wires encapsulated in carbon nanotubes, J. Phys.: Cond. Matt. 23 (26) (2011) 265302.

[19] T. Fujimori, R. dos Santos, T. Hayashi, M. Endo, K. Kaneko, D. Tománek, Formation and properties of selenium double-helices inside double-wall carbon nanotubes: experiment and theory, ACS Nano 7 (2013) 5607–5613.

[20] H.-P. Komsa, R. Senga, K. Suenaga, A. V. Krasheninnikov, Structural distortions and charge density waves in iodine chains encapsulated inside carbon nanotubes, Nano Lett. 17 (6) (2017) 3694–3700.

[21] R. Ripan, I. Ceteanu, Chimia metaleor, Vol. 2, Editura didactică si pedagogică, Bucharest, 1966, translated under the title *Neorganicheskaya khimia*, Moscow, Mir, 1972, vol. 2, p. 189.

[22] H. Yu, C. Lu, T. Xi, L. Luo, J. Ning, C. Xiang, Thermal decomposition of the carbon nanotube/sio$_2$ precursor powders, J. Therm. Anal. Calorim. 82 (1) (2005) 97–101.

[23] X. Wei, M.-S. Wang, Y. Bando, D. Golberg, Thermal stability of carbon nanotubes probed by anchored tungsten nanoparticles, Sci. Technol. Adv. Mater. 12 (4) (2011) 044605.

[24] Yusuke Nakanishi, Yung-Chang Lin, Zheng Liu, Shuwen Wang, and Katsumi Kaneko (private communication).

[25] E. Lavut, B. Timofeyev, V. Yuldasheva, G. Galchenko, Enthalpy of formation of niobium pentachloride, J. Chem. Thermodyn. 14 (6) (1982) 531–535.

[26] P. Gross, C. Hayman, D. L. Levi, G. L. Wilson, The heats of formation of metal halides. niobium and tantalum pentachlorides, Trans. Faraday Soc. 56 (1960) 318–321.

[27] S. Harjanto, A. Shibayama, K. Sato, G. Suzuki, T. Otomo, Y. Takasaki, T. Fujita, Thermal decomposition of NbCl$_5$ in reductive atmosphere by using hydrogen gas, Resour. Process. 52 (3) (2005) 113–121.

[28] M. D. Korzyński, L. Braglia, E. Borfecchia, C. Lamberti, M. Dincă, Molecular niobium precursors in various oxidation states: An XAS case study, Inorg. Chem. 57 (21) (2018) 13998–14004.

[29] W. Gu, J. Bai, B. Dong, X. Zhuang, J. Zhao, C. Zhang, J. Wang, K. Shih, Catalytic effect of graphene in bioleaching copper from waste printed circuit boards by acidithiobacillus ferrooxidans, Hydrometallurgy 171 (2017) 172–178.

[30] X. Xu, Y. Liu, Z. Liu, F. Ke, C. Lin, K. Liu, Z. Zhang, Z. Hu, X. Li, X. Guo, Pristine graphene as a catalyst in reactions with organics containing C=O bonds, arXiv:1707.05607 (2017).

[31] R. Tran, Z. Xu, B. Radhakrishnan, D. Winston, W. Sun, K. A. Persson, S. P. Ong, Surface energies of elemental crystals, Sci. Data 3 (2016) 160080.

[32] K. C. Mills, Y. C. Su, Review of surface tension data for metallic elements and alloys: Part 1-pure metals, Int. Mater. Rev. 51 (6)

(2006) 329–351.

[33] E. N. Hodkin, M. G. Nicholas, D. M. Poole, The surface energies of solid molybdenum, niobium, tantalum and tungsten, J. Less Common Met. 20 (2) (1970) 93–103.

[34] W. L. McMillan, Transition temperature of strong-coupled superconductors, Phys. Rev. 167 (1968) 331–344.

[35] E. Artacho, E. Anglada, O. Dieguez, J. D. Gale, A. Garcia, J. Junquera, R. M. Martin, P. Ordejon, J. M. Pruneda, D. Sanchez-Portal, J. M. Soler, The siesta method; developments and applicability, J. Phys. Cond. Mat. 20 (6) (2008) 064208.

[36] J. P. Perdew, K. Burke, M. Ernzerhof, Generalized gradient approximation made simple, Phys. Rev. Lett. 77 (1996) 3865–3868.

[37] N. Troullier, J. L. Martins, Efficient pseudopotentials for plane-wave calculations, Phys. Rev. B 43 (1991) 1993.

[38] H. J. Monkhorst, J. D. Pack, Special points for brillouin-zone integrations, Phys. Rev. B 13 (1976) 5188–5192.

[39] M. R. Hestenes, E. Stiefel, Methods of conjugate gradients for solving linear systems, J. Res. Natl. Bur. Stand. 49 (1952) 409–436.